

## **PHASE TRANSFORMATIONS AND INHERITED ODFs : IMPLICATIONS FOR PETROPHYSICAL PROPERTIES**

**D. MAINPRICE**

Laboratoire de Tectonophysique  
Université de Montpellier II, 34095 Montpellier Cedex 05 - France

**M. HUMBERT and F. WAGNER**

Laboratoire de Métallurgie des Matériaux Polycrystallins  
Université de Metz, 57045 Metz Cedex - France

### **INTRODUCTION**

Seismic discontinuities in the Earth's mantle have been interpreted as phase transformations (1). Little attention has been paid to the three dimensional nature of seismic properties of regions undergoing phase transformation or the anisotropy of the petrophysical properties of such regions. Recent progress in anisotropic seismic tomography (2) reveals the need for a better understanding of the anisotropic rock properties. Potentially the knowledge of anisotropic properties will add a further constraint for the development of more realistic large scale geodynamic models.

### **PHASE TRANSFORMATIONS**

The mechanisms phase transformation can be complex, we can to a first approximation classify the mechanisms into two classes.

1. Nucleation & Growth, a mechanism which depends on a nucleation event and diffusion controlled growth process. The nucleation is usually heterogeneous on imperfections. Depending on the anisotropy of crystal structure and the thermodynamic conditions this mechanism may or may not result in an orientation relationship between "old" and "new" phases.

2. Martensitic mechanism is a diffusionless transformation. The crystal structure of the "old" phase is sheared in systematic coordinated manner such that any atom is moved by less than one atomic spacing. Martensitic transformation results in changes of crystal structure, but not composition. Such transformation always produce a fixed orientation relationship between the "old" and "new" phase.

### **DESCRIPTION OF ORIENTATION RELATIONSHIPS**

It is traditional in quantitative texture analysis to describe the orientations of an ensemble of grains by the Orientation Distribution Function (ODF) (3). The orientation of an individual grain (crystal) may be defined by three Euler angles ( $\varphi_1$ ,  $\phi$ ,  $\varphi_2$ ) which

describe the rotation between the crystal and specimen reference frames. In a similar manner one can define the orientation ( $\Delta g$ ) of the "old" phase reference with respect to "new" phase (fig.1). Using such a description of the orientation relationships it is easy to show that the orientation of the new phase is given by

$$\begin{pmatrix} \text{new} \\ g_n \end{pmatrix} = \Delta g \cdot S_n^{\text{old}} \cdot g^{\text{old}}$$

where  $S_n^{\text{old}}$  is the n symmetry operations of the old phase and  $g^{\text{old}}$  is the "old" phase orientation. Using such an approach we have calculated the ODF of the "new" phase using the ODF of the "old" phase, the symmetry operations and the know orientation relationships ( $\Delta g$ ).

### CALCULATION OF PETROPHYSICAL PROPERTIES

Given the appropriate tensor transformation law (4) we can rotate the petrophysical constants into their orientation in sample coordinates. For the case of triclinic crystal and specimen symmetry the average polycrystal tensor ( $\bar{T}$ ) can be determined by integration as

$$\bar{T} = \int T(g) \cdot f(g) \cdot dg$$

$$dg = \frac{1}{8\pi} \sin \Phi \, d\phi_1 \, d\Phi \, d\phi_2$$

where  $T(g)$  is the tensor in sample coordinates and  $f(g)$  the ODF. The familiar Voigt, Reuss or Voigt-Reuss-Hill averages may be calculated in this manner.

### ALPHA-BETA QUARTZ TRANSITION

The alpha-beta quartz transition is a good test case for the method presented here because all the petrophysical constants have been determined. We have used the ODF of an alpha-quartz polycrystal (fig.2) quartzite GRAN133 (5) which is known to have experienced  $\beta$ -quartz stability conditions (granulite metamorphic facies).

For the extraction of hydrothermal energy, thermal cracking of the source region is an important process for producing permeability in granites and quartzites. The anisotropy of thermal expansion, elastic properties and the temperature change are the important parameters which determine the degree and orientation of thermal cracks. The thermal expansion of a quartz single crystal and polycrystal GRAN133 (fig.3) have been calculated using the data of Skinner (6). The minimum thermal expansion occurs parallel to the c-axes. The smoothness of the distribution of thermal expansion is due to the second order nature of this tensor property.

We have undertaken a simimar calculation for the compressional seismic velocity ( $V_p$ ) as a function of temperature for GRAN133 (fig. 4) using the single crystal elastic constants of McSkimin et al. (7), Zubor and Firsova (8), Kammer et al. (9) to cover the temperature range. The calculated  $V_p$  can be compared with experimental determination by Kern (10) on a quartzite with a weak texture. The calculations agree well with the experimental results except that the minimum velocity, associated with the

transition is displaced by 80°C. The shift in the experimental minimum is due to internal stresses generated by the anisotropic thermal expansion. The differential stresses cause a shift of the transition temperature (11).

#### OLIVINE-SPINEL TRANSITION

Various models have been proposed for the olivine- $\rightarrow$  $\beta$ -spinel transition in recent years. The transition is thought to be responsible for the major seismic discontinuity in compressional ( $V_p$ ) and shear wave ( $V_s$ ) velocities at 400 km depth in the Earth's Mantle. As an illustration of the potential of the method described here we will model the transition using the crystallographic relationships for  $\Delta g$  proposed by Madon and Poirier (12) from which

$$\begin{aligned} & (1\ 0\ 0) \text{ olivine} // (1\ \bar{1}\ 0) \beta\text{-spinel} \\ & [0\ 0\ 1] \text{ olivine} // [0\ 0\ 1] \beta\text{-spinel} \end{aligned}$$

For the ODF of the "old" or olivine phase we have used an ODF calculated from a kimberlite nodule (Bulfontein, South Africa) extracted from a depth of 140 km in the Upper mantle (13). The calculated pole figures for the  $\beta$ -spinel (fig. 5) show the alignment of [001] olivine and [001] spinel. The calculated  $V_p$  for olivine show a maximum which corresponds to maximum of [100] axes (the fast  $V_p$  direction), similarly the calculated  $V_p$  for  $\beta$ -spinel shows a maximum which corresponds to a maximum of [010] axes. Note that the maximum velocities in the olivine and spinel polycrystals are not parallel but rotated by 90°, indicating a fundamental change in the orientation of the seismic anisotropy at the transition.

The composition of the Mantle is currently the subject of much speculation. At the 400 km depth the composition has been estimated to be either 70% olivine (1) or 40% olivine (14). Seismic observations suggest that velocity jump ( $\Delta V_p$ ) at 400 km for  $V_p$  is

$$3.5\% < \left( \frac{\Delta V_p}{V_p} \right)_{\text{obs}} < 6\%$$

according to Montagner and Anderson (2). If the transition occurs over a small depth interval (less than 10 km) (15) we can assume that only phase transformation contributing to  $\Delta V_p$  is the olivine- $\rightarrow$  $\beta$ -spinel. It is reasonable to estimate the volume fraction of olivine ( $X_{O1}$ ) in the transition zone by

$$X_{O1} = \frac{(\Delta V_p/V_p)_{\text{obs}}}{(\Delta V_p/V_p)_{\alpha-\beta}}$$

where  $(\Delta V_p/V_p)_{\text{obs}}$  is given by Montagner and Anderson (2) and  $(\Delta V_p/V_p)_{\alpha-\beta}$  is the velocity change for a pure olivine aggregate transforming to  $\beta$ -spinel. Using such an approach will give values of between 56% <  $X_{O1}$  < 96% for propagation directions along X in fig. 5 or 19% <  $X_{O1}$  < 33% for propagation along Z. We suggest that it is important to take into account the propagation direction when undertaking such evaluations.

## CONCLUSIONS

1. A quantitative calculation of the petrophysical properties of a transformed polycrystal is possible.
2. The seismic properties "above" and "below" the phase transformation (e.g. 400 km, olivine-spinel) can be used to characterize an interface or reflector.
3. Further constraints on the Earth's Mantle composition may be possible with ;
  - a) control of the propagation direction in seismic data
  - b) crystallographic characterization of the transformation under Mantle conditions (low stress, high temperature and pressure).

## ACKNOWLEDGEMENTS

Financial support to D.M. from the CNRS/INSU DBT-Geodynamics program is gratefully acknowledged.

## REFERENCES

1. Ringwood, A.E. Composition and Petrology of the Earth's Mantle p.618 (McGraw-Hill, New York, 1975).
2. Montagner, J.P. & Anderson, D.L. *Phys.Earth Planet.Int.* **58**, 205-227 (1989).
3. Bunge, H.J. *Texture analysis in Materials Science* p.593 (Butterworths, London, 1982).
4. Nye, J.F. *Physical properties of crystals. Their representation by tensors and matrices* p.322 (Clarendon Press, Oxford, 1957).
5. Schmid, S.M., Casey, M. & Starkey, J. *Tectonophysics* **78**, 101-117 (1981).
6. Skinner, B.J. in *Handbook of Physical Constants* (ed. S.P. Clark, Jr.) 75-96 (Geol. Soc. Am. Bull., 1966).
7. McSkimin, H.J., Anreatch, J.R. & Thurston, R.N. *J. Appl. Phys.* **36**, 1624-1632 (1965).
8. Zubov, V.G. & Firsova, M.M. *Soviet Phys.-Cryst., English Transl.* **7**, 374-376 (1962).
9. Krammer, E.W., Pardue, T.E. & Frissel, H.F. *J. of Applied Phys.* **19**, 265-270 (1948).
10. Kern, H. *Phys. Chem. Mineral.* **4**, 161-171 (1979).
11. Coe, R.S. & Paterson, M.S. *J. Geophys. Res.* **74**, 4921-4948 (1969).
12. Madon, M. & Poirier, J.P. *Phys. Earth Planet. Int.* **33**, 31-44 (1983).
13. Boullier, A.M. *Structure des peridotites enclaves dans les kimberlites d'Afrique de Sud* (Université de Nantes, 1975).
14. Anderson, D.L. & Bass, J.D. *Nature* **320**, 321-328 (1986).
15. Bina, C.R. & Wood, B.J. *J.Geophys.Res.* **92**, 4853-4866 (1987).

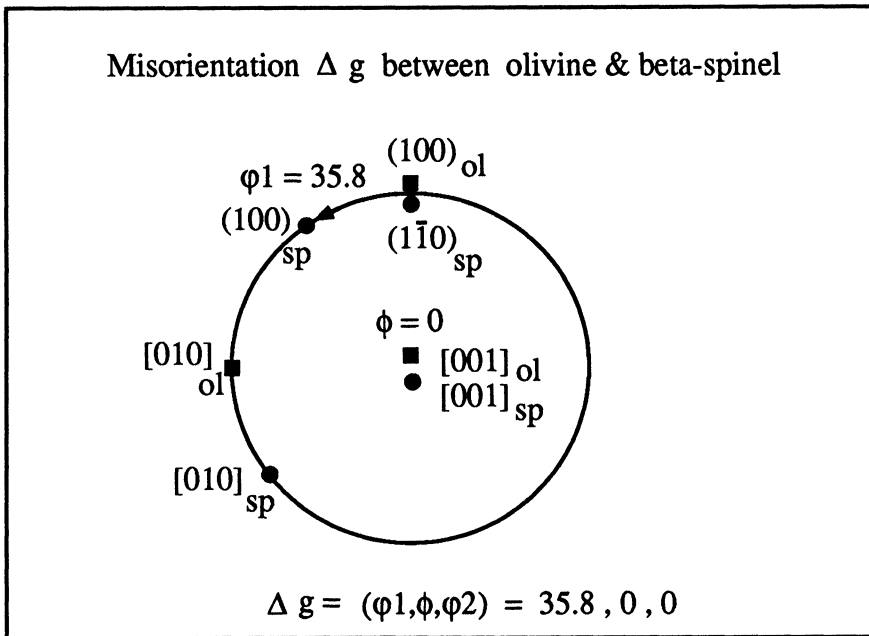


FIGURE 1. Euler angle description of misorientation between phases

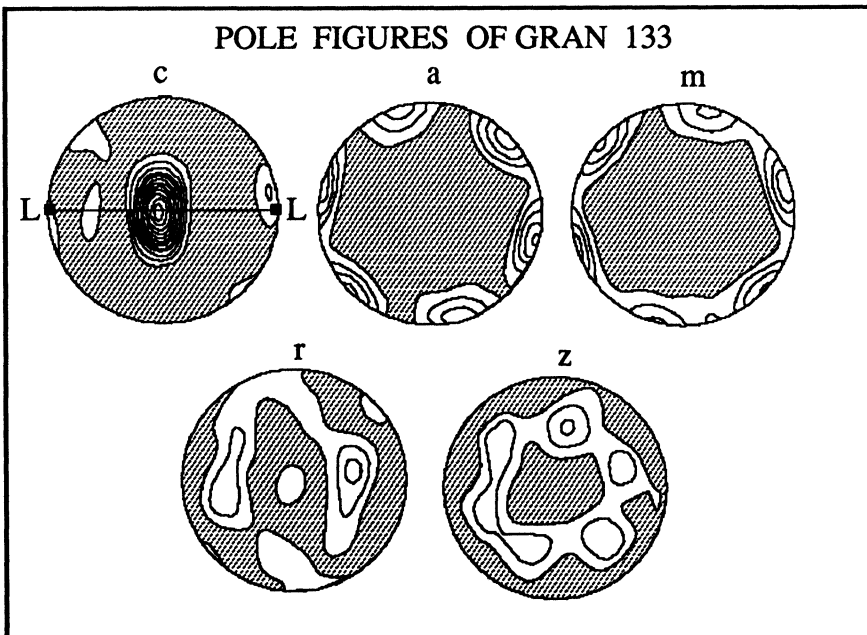


FIGURE 2. Polefigures of quartzite GRAN 133 recalculated from ODF

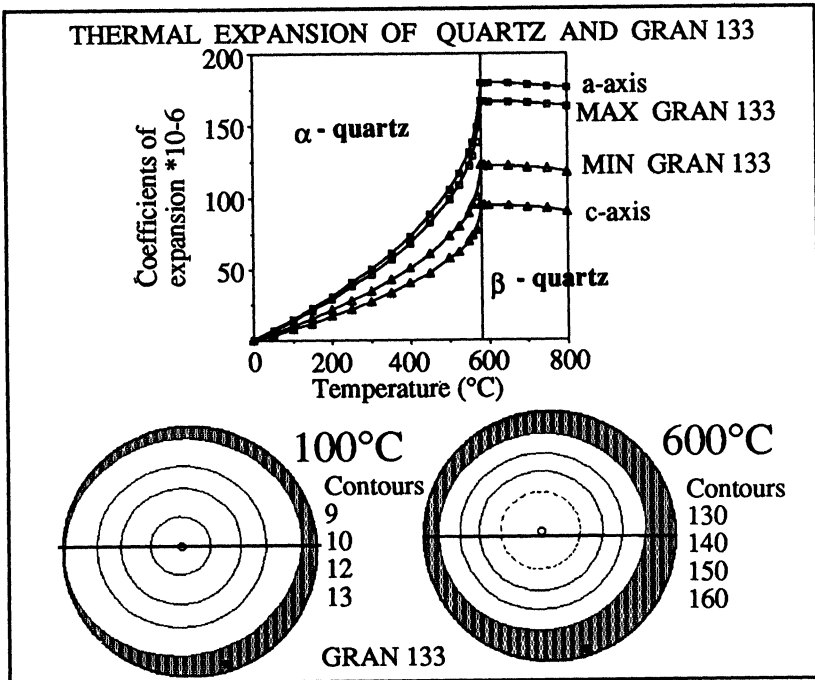


FIGURE 3. Thermal expansion for GRAN 133 calculated from ODF

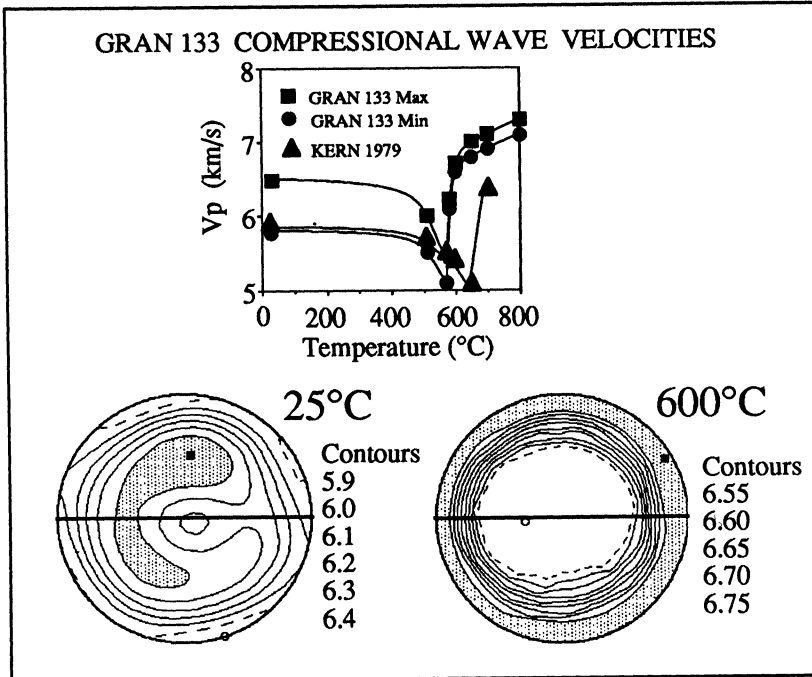


FIGURE 4. Compressional wave velocities for GRAN 133 calculated from ODF

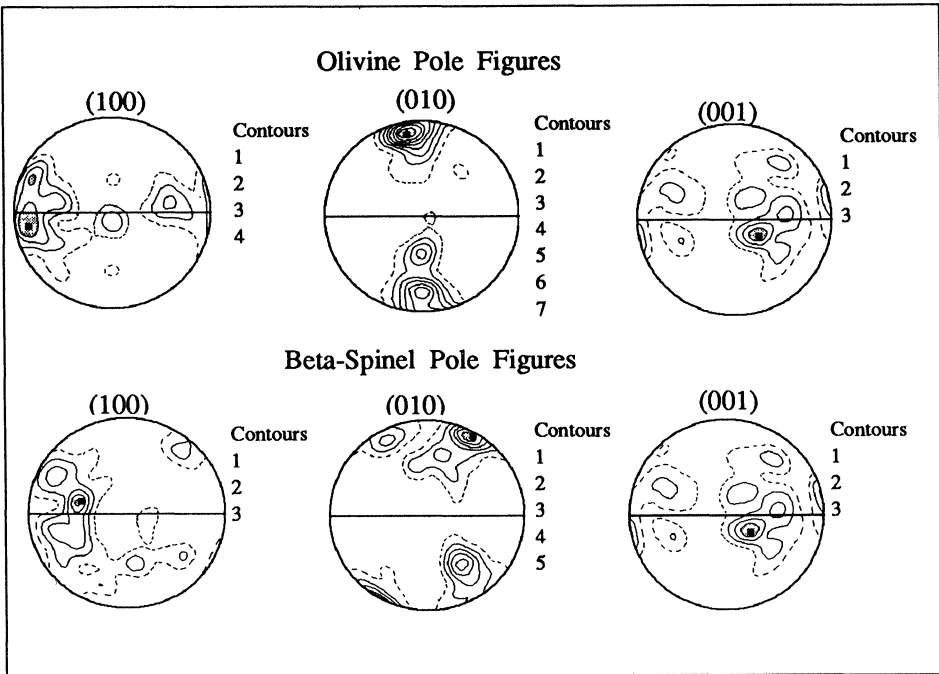


FIGURE 5. Olivine and Beta-Spinel pole figures recalculated from ODF

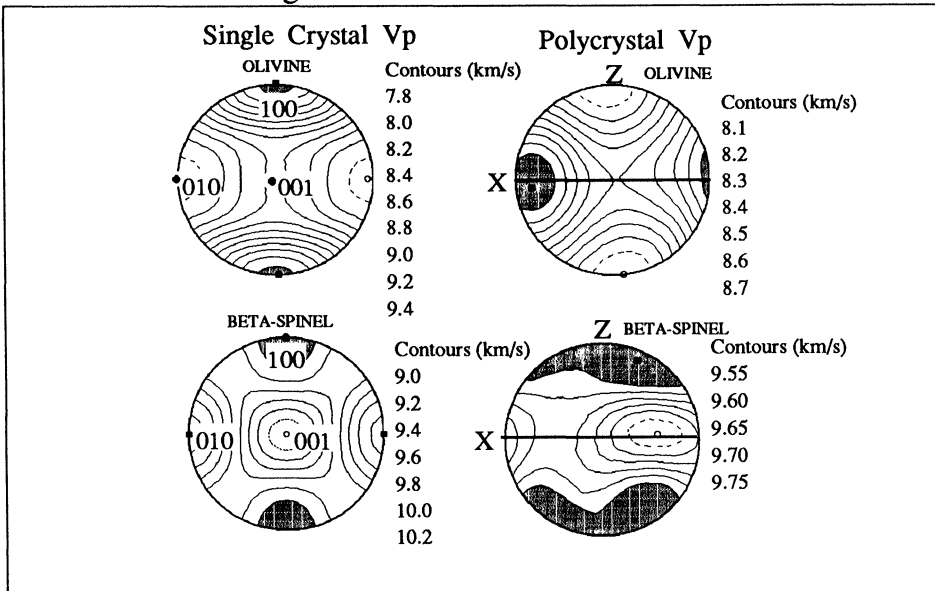


FIGURE 6. Compressional wave velocities for single crystal and polycrystalline olivine and beta-spinel